Solid-State NMR Determination of Sugar Ring Pucker in ^{13}C-Labeled 2′-Deoxynucleosides

Lorens van Dam,* Niels Ouwerkerk,† Andreas Brinkmann,* Jan Raap,† and Malcolm H. Levitt*‡
*Physical Chemistry, Arrhenius Laboratory, Stockholm University, 106 91 Stockholm, Sweden, †Leiden Institute of Chemistry, Leiden University, 2300 RA Leiden, The Netherlands, and ‡Chemistry Department, Southampton University, Southampton SO17 1BJ, United Kingdom

ABSTRACT The H3′–C3′–C4′–H4′ torsional angles of two microcrystalline 2′-deoxynucleosides, thymidine and 2′-deoxycytidine·HCl, doubly ^{13}C-labeled at the C3′ and C4′ positions of the sugar ring, have been measured by solid-state magic-angle-spinning nuclear magnetic resonance (NMR). A double-quantum heteronuclear local field experiment with frequency-switched Lee–Goldberg homonuclear decoupling was used. The H3′–C3′–C4′–H4′ torsional angles were obtained by comparing the experimental curves with numerical simulations, including the two ^{13}C nuclei, the directly bonded ^{1}H nuclei, and five remote protons. The H3′–C3′–C4′–H4′ angles were converted into sugar pucker angles and compared with crystallographic data. The δ torsional angles determined by solid-state NMR and x-ray crystallography agree within experimental error. Evidence is also obtained that the proton positions may be unreliable in the x-ray structures. This work confirms that double-quantum solid-state NMR is a feasible tool for studying sugar pucker conformations in macromolecular complexes that are unsuitable for solution NMR or crystallography.

INTRODUCTION

The conformations of individual monomers in the polynucleic acids DNA and RNA are decisively important for their biological function. In particular, protein-DNA recognition is thought to involve the detailed local conformation of the DNA molecule through the so-called indirect recognition mechanism (Travers, 1993). Spectroscopic methods that are capable of obtaining information on the individual nucleotide conformations are therefore most important, particularly if they are applicable to large macromolecular assemblies.

A particularly important conformational parameter in nucleotides, nucleosides, and nucleic acids is the angle δ, defined as the torsional angle C5′–C4′–C3′–O3′ of the ribofuranose unit (Fig. 1). Together with the pucker amplitude, which is highly conserved in nucleosides (see Saenger, 1984, page 55), the torsional angle δ defines the pucker of the ribofuranose ring, which affects the entire nucleotide fragment and potentially the conformation of adjacent units. For instance, the sugar pucker changes from C2′-endo to C3′-endo in the transition from the B-form to the A-form of DNA, representing a change in δ from around *gauche* (60°) to around *trans* (180°).

The principal methods for examining nucleotide conformations are x-ray crystallography, solution NMR, and solid-state NMR. High-resolution x-ray crystallography gives direct information on the molecular structure. Solution-state NMR, in contrast, gives indirect information on the torsional angles through chemical shifts (Santos et al., 1989; Gorenstein, 1992; Xu et al., 1998; Rossi and Harbison, 2001), scalar J-couplings (Davies, 1978; Ippel et al., 1996), and cross-correlated relaxation effects (Boisbouvier et al., 2000; Felli et al., 1999). However, as the DNA and RNA molecules grow larger, and for the interesting cases of polynucleotide–protein complexes, both x-ray crystallography and solution-state NMR frequently encounter difficulties, the former due to imperfect crystallization, and the latter because of spectral line broadening due to slow molecular rotation.

Solid-state NMR does not require long-range crystallinity or rapid molecular motion. Several solid-state NMR methods have found application in the structural investigations of nucleic acids (Alam and Drobny, 1991; Lee et al., 2000; van Dam and Levitt, 2000). In particular, the torsional angle δ may be estimated from isotropic ^{13}C chemical shift values (Santos et al., 1989; Rossi and Harbison, 2001). However, chemical shift information can be difficult to interpret in structured macromolecules due to nonlocal effects, so a complementary method for estimating δ would be useful.

Torsion angles may also be estimated by solid-state NMR, if experiments are used that are sensitive to the relative orientations of nuclear spin interaction tensors (Feng et al., 1996; Ishii et al., 1996; Schmidt-Rohr, 1996a,b; Tycko et al., 1996; Weliky and Tycko, 1996; Costa et al., 1997; Feng et al., 1997; Fujiwara et al., 1997; Gregory et al., 1997; Hong et al., 1997; Feng et al., 1998; Bower et al., 1999; Feng et al., 2000; Middleton et al., 2000; Ravindranathan et al., 2000; Takegoshi et al., 2000). A particular useful class of experiments is called double-quantum heteronuclear local field (2Q-HLF) spectroscopy. These experiments exploit the evolution of a correlated two-spin state, double-quantum coherence (2QC), under the heteronuclear

Submitted March 22, 2002, and accepted for publication July 10, 2002.

Dr. Brinkmann's present address is Physical Chemistry, Univ. of Nijmegen, 6525ED, The Netherlands.

Address reprint requests to Malcolm H. Levitt, Chemistry Department, Southampton University, University Rd., Southampton SO17 1BJ, U.K. Tel.: +44-23-80596753; Fax: +44-23-80593781; E-mail: mhl@soton.ac.uk.

0006-3495/02/11/2835/10 $2.00

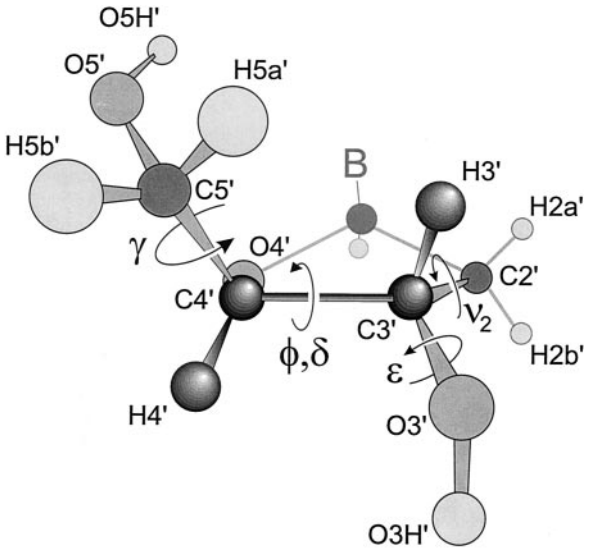

FIGURE 1 The structure and atomic labeling scheme of the sugar unit in a nucleoside, showing the relevant torsional angles.

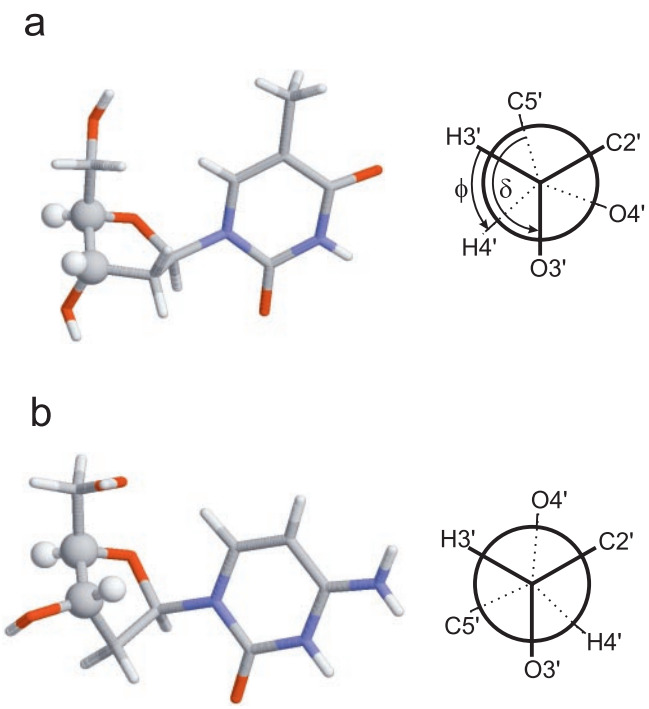

FIGURE 2 Crystal structures of (*a*) thymidine and (*b*) 2′-deoxycytidine hydrochloride, showing 2′-endo (or S-type) and 3′-endo (or N-type) sugar puckers, respectively (see Chekhlov, 1995 and Subramanian and Hunt, 1970). The H3′, C3′, C4′, and H4′ atoms are shown as balls. The torsion angles H3′–C3′–C4′–H4′ (ϕ) and C5′–C4′–C3′–O3′ (δ) are indicated by Newman projections. The chloride atom has been omitted from (*b*), for the sake of clarity.

local fields of neighboring spins. The evolution of the 2QC is sensitive to the correlation of the heteronuclear local fields, and therefore to the relative orientation of the heteronuclear dipolar coupling tensors. In particular, the HCCH-2Q-HLF experiment was designed to measure the torsional angle in an $^{1}H–^{13}C–^{13}C–^{1}H$ molecular fragment by allowing ^{13}C 2QC to evolve under the $^{13}C–^{1}H$ heteronuclear dipolar couplings (Feng et al., 1996). This experiment has found several applications in biologically relevant molecules. For example, the H–C10–C11–H molecular torsional angle in the isomerization region of the retinal chromophore was determined in the ground state of rhodopsin (Feng et al., 1997) and in the metarhodopsin-I photointermediate (Feng et al., 2000). The HCCH-2Q-HLF experiment has also been applied to mono and disaccharides (Ravindranathan et al., 2000, 2001), the drug compound cimetidine (Middleton et al., 2000) and bacteriorhodopsin (Lansing et al., 2002).

The HCCH-2Q-HLF experiment is an appropriate spectroscopic tool for studying nucleic acid conformations because each of the C4′ and C3′ sites has one attached proton, and selective ^{13}C labeling of the C4′ and C3′ sites is technically feasible using known synthetic routes (Ouwerkerk et al., 2000, 2002). An attractive feature of the 2Q-HLF experiment is that NMR signals from the natural abundance ^{13}C background are effectively suppressed, making the experiment feasible even in large molecular assemblies. The information provided by this experiment is complementary to that provided by chemical shift data. In preparation for experiments on macromolecular nucleic acid complexes, we have first applied the method to two different microcrystalline $^{13}C_2$-labeled nucleosides, where a direct comparison with x-ray structures may be made. This comparison is the subject of this paper.

HCCH-2Q-HLF spectroscopy was performed to determine the H3′–C3′–C4′–H4′ torsion angles in two $^{13}C_2$-labeled microcrystalline 2′-deoxynucleosides, [3′,4′-$^{13}C_2$]-thymidine and [3′,4′-$^{13}C_2$]-2′-deoxycytidine hydrochloride. The x-ray structure of thymidine (Young et al., 1969; Chekhlov, 1995) shows a 2′-endo or S-type sugar ring pucker that can be described as an intermediate between the $^{2}_{1}T$ and ^{2}E conformation (Altona, 1982; Saenger, 1984), see Fig. 2 *a*. The x-ray structure of 2′-deoxycytidine, in contrast, displays a C3′-endo or N-type sugar pucker characterized by a $^{3}_{4}T$ conformation (Altona, 1982; Saenger, 1984), see Fig. 2 *b*. The different sugar puckers in these two nucleosides provide us with a good test of the 2Q-HLF experiment.

The HCCH-2Q-HLF experiments provide a direct measure of the H3′–C3′–C4′–H4′ torsional angle ϕ. However, to obtain an estimate of the C5′–C4′–C3′–O3′ torsional angle δ, assumptions must be made about the local geometry of the near-tetrahedral C3′ and C4′ sites. In this paper, we obtain estimates of the geometrical parameters and their confidence limits by a statistical analysis of published neutron diffraction structures. The inferred torsional angles δ for [3′,4′-$^{13}C_2$]-thymidine and [3′,4′$^{13}C_2$]-2′-deoxycytidine·HCl are compared with the x-ray diffraction values. We find that the NMR and x-ray estimates of the δ

torsional angles are in good agreement, providing that the influence of neighboring protons is taken into account when analyzing the solid-state NMR data. At the same time, we find evidence that the proton positions do not coincide with the hydrogen atom positions reported in the x-ray structures.

MATERIALS AND METHODS

Samples

The two $^{13}C_2$-labeled nucleosides [3′,4′-$^{13}C_2$]-thymidine and [3′,4′-$^{13}C_2$]-2′-deoxycytidine were synthesized by methods described elsewhere (Ouwerkerk et al., 2000, 2002).

Crystalline [3′,4′-$^{13}C_2$]-thymidine was prepared by slow evaporation of an aqueous solution of the synthetic $^{13}C_2$-labeled 2′-deoxynucleoside (Young et al., 1969). The quality of the single crystals was checked by x-ray analysis (Lutz et al., 2001). The crystals were washed with a drop of water and crushed in a mortar. In the following discussion, [3′,4′-$^{13}C_2$]-thymidine is referred to as $^{13}C_2$-dT.

The [3′,4′-$^{13}C_2$]-2′-deoxycytidine hydrochloride salt was prepared by addition of 1.05 equivalent of 1 M HCl to the neutral-labeled compound. The crystals obtained by slow evaporation of an aqueous solution of this compound appeared to be inhomogeneous, as indicated by a complex line pattern of the magic-angle solid-state ^{13}C-NMR spectrum. After several unsuccessful attempts to improve the crystallization conditions, we decided to use the powder obtained by lyophilization. The magic-angle solid-state ^{13}C-NMR spectrum of the lyophilized powder showed two well-resolved signals at chemical shifts 66.2 and 86.5 ppm (referenced to the lower-shift peak of ademantane at 28.5 ppm), which are appropriate for the 3′ and 4′ sites (data not shown). The structure of the lyophilized powder was further analyzed by means of x-ray diffraction using a Philips PW 1050 diffractometer and K_α radiation. For the region between $2\theta = 0°–40°$, the experimental diffraction pattern agreed well with the theoretical pattern calculated from the literature crystal data (Subramanian and Hunt, 1970). We conclude that the lyophilized powder is microcrystalline with a structure identical to that of the published crystals. This conclusion is supported by the solid-state NMR results reported below. In the following discussion, [3′,4′-$^{13}C_2$]-2′-deoxycytidine is referred to as $^{13}C_2$-dC·HCl.

Solid-state NMR

A Varian CMX Infinity system equipped with a 4.7 Tesla superconducting magnet was used. The ^{13}C resonance frequency was −50.34 MHz. All experiments were done using a standard 4-mm Varian Apex II MAS probe. The nucleoside crystals were finely ground and placed in the center of the rotor. The remaining space at the edges of the rotor was filled by teflon spacers. In all experiments, 4000 Hz magic-angle-spinning was applied with a stability of ±1 Hz. The temperature was −85°C for the $^{13}C_2$-dT sample and room temperature (ambient) for the $^{13}C_2$-dC·HCl sample. A low temperature was used for the thymidine sample to reduce the spin-lattice relaxation time, which is inconveniently long at room temperature. Cross-polarization magic-angle spinning spectra were acquired using a standard RAMP-CP sequence (Metz et al., 1994).

The HCCH torsional angle estimations used a modified 2Q-HLF pulse-sequence, based on the original implementation (Feng et al., 1996) (Fig. 3). This sequence assumes that the rf (reference frequency) is set to the mean value of the two isotropic shift frequencies, to avoid chemical shift evolution of the double-quantum coherences. The sequence starts with ramped cross polarization (Metz et al., 1994) to enhance the ^{13}C magnetization. The following ^{13}C rf-pulse converts the transverse magnetization into longitudinal ^{13}C magnetization. The homonuclear double-quantum recoupling sequence POST-C7 (Hohwy et al., 1998) of duration τ_{2Q} converts the sum longitudinal magnetization into homonuclear 2QC. The excited 2QC

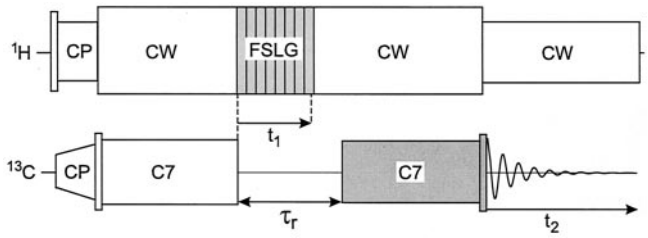

FIGURE 3 The 2Q-HLF pulse sequence with FSLG homonuclear ^{1}H decoupling.

is allowed to evolve for one rotation period, τ_r, this constant interval being divided into two parts. The first part t_1, is occupied by a homonuclear decoupling sequence, applied on the abundant spin species ^{1}H. In this work, we achieved homonuclear decoupling using the frequency-switched Lee–Goldberg (FSLG) method, which has been shown to perform particularly well in a heteronuclear context (Bielecki et al., 1989). The second part is an interval τ_r–t_1 during which unmodulated high-power proton irradiation is applied to decouple the heteronuclear ^{13}C–^{1}H interactions. A series of experiments is acquired in which t_1 is incremented from zero up to a complete rotor period. The 2QC is converted into longitudinal magnetization by the reconversion sequence of duration τ_{2Q}. The longitudinal magnetization is converted into observable magnetization by a $\pi/2$ read pulse. The ^{13}C NMR signal is detected in the subsequent period t_2.

Two hundred and fifty-six complex points were acquired in the t_2-dimension during a total acquisition time of 21.3 ms and a repetition delay of 4 s. The time-domain data were zero-filled to 512 points, Fourier transformed, and zero-order phase-corrected. The FSLG decoupling used a ^{1}H nutation frequency of 78 kHz and a frequency jump of ±55.4 kHz around the center of the ^{1}H spectrum. The frequency jumps were performed with a simultaneous π phase shift every 10.4 μs. The ^{1}H CW decoupling nutation frequency was 125 kHz during the C7 and τ_r–t_1 interval, and 74 kHz during the ^{13}C acquisition interval. The interval τ_{2Q} was set to 642.8 μs.

RESULTS

Cross-polarization magic-angle spinning spectra

The cross-polarization magic-angle spinning spectra of $^{13}C_2$-dT and $^{13}C_2$-dC·HCl both displayed two well-resolved ^{13}C peaks. The ^{13}C chemical shift values were 72.0 ppm (C3′) and 86.6 ppm (C4′) for $^{13}C_2$-dT, and 66.2 ppm (C3′) and 86.5 ppm (C4′) for $^{13}C_2$-dC·HCl (in both cases, the most shielded ^{13}C peak of adamantane was used as a 28.5 ppm external reference). The chemical shifts are in good agreement with values reported in the literature (Leupin et al., 1987; Santos et al., 1989; Xu et al., 1998), and already suggest a difference in sugar pucker of the two compounds.

Double-quantum-filtered ^{13}C spectra

Double-quantum-filtered spectra were acquired using the pulse sequence in Fig. 3, omitting the central τ_r interval. The measured 2Q-filtering efficiency obtained with the POST-C7 pulse sequence (Hohwy et al., 1998) was 57% for both samples, which compares favorably with the theoretical limit of 73% (Lee et al., 1995).

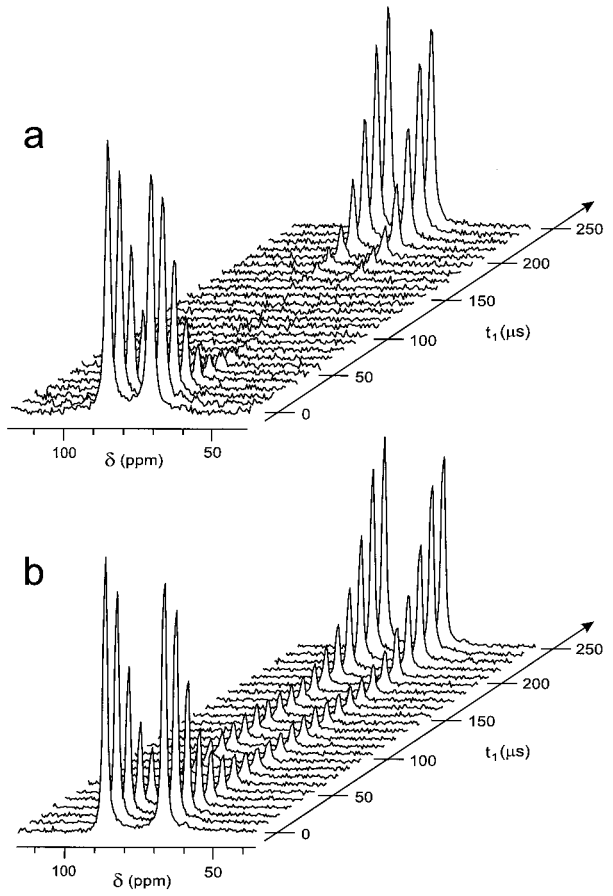

FIGURE 4 Experimental 2Q-HLF spectra of (*a*) [3′,4′-$^{13}C_2$]-thymidine and (*b*) [3′,4′-$^{13}C_2$]-2′-deoxycytidine·HCl, as a function of the evolution interval t_1.

HCCH-2Q-HLF spectroscopy

Figure 4 shows the experimental 2Q-filtered ^{13}C signals for (*a*) $^{13}C_2$-dT and (*b*) $^{13}C_2$-dC·HCl as a function of the evolution interval t_1. In both cases, the signals initially decay rapidly as t_1 is increased, but recover almost completely when t_1 approaches a full rotor period. This behavior is indicative of efficient homonuclear decoupling under the FSLG sequence.

Differences in the t_1 dependence of these signals are evident from these plots. The $^{13}C_2$-dT signals decay to a value close to zero when t_1 is in the vicinity of one half of a rotor period, whereas the $^{13}C_2$-dC·HCl signals remain visible at all t_1 values. This behavior is due to the different sugar pucker angles for the two nucleosides.

DATA ANALYSIS

Simulations of the 2Q evolution curves

As described in Feng et al. (1996), the torsional angle ϕ of the H–^{13}C–^{13}C–H fragment may be estimated by fitting the total integrated intensity of the ^{13}C signals under the 2Q-HLF pulse-sequence to calculated functions $Af(t_1, \kappa,\phi)e^{-\lambda t_1}$, where A and λ are fit parameters, and the theoretical 2Q evolution curve is

$$f(t_1, \kappa, \phi) = 2^{1-N}\Big\langle \sin^2(\omega_{2Q}\tau_{2Q}) \times \sum_{m_1,m_2\ldots m_N} \cos \Phi^{m_1,m_2\ldots m_N}(t_1, \kappa, \phi)\Big\rangle. \quad (1)$$

Here, N is the number of protons included in the simulation, and the summation is taken over all combinations of proton spin states, e.g., $(m_1, m_2) = (+½, +½), (-½, +½), (+½, -½), (-½, -½)$ in the case of two protons. ω_{2Q} is the ^{13}C–^{13}C 2Q nutation frequency under the C7 pulse sequence (which is dependent on the relative orientation of the internuclear vector with respect to the rotor axis, see Lee et al., 1995) and τ_{2Q} is the 2Q excitation and reconversion interval. κ is the scaling factor of the homonuclear ^1H decoupling sequence, and the angular brackets signify a powder average over molecular orientations. In practice, the computations used 3722 crystallite orientations selected according to the Zaremba–Cheng–Wolfsberg (ZCW) method (Cheng et al., 1973). Using roughly twice as many orientations made no difference to the outcome.

The phase function Φ is given by (Feng et al., 1996)

$$\Phi^{m_1,m_2\ldots m_N}(t_1, \kappa, \phi) = 2\kappa \int_0^{t_1} \sum_{i=1}^{N} m_i(\omega_{i3'}(t, \phi) + \omega_{i4'}(t, \phi))\, dt, \quad (2)$$

where i is an index for the protons included in the simulation and the labels 3′ and 4′ refer to the ^{13}C sites. The through-space dipole–dipole coupling frequency between sites i and j is given by

$$\omega_{ij}(t, \phi) = \sum_{m',m} b_{ij} D^2_{0m'}(\Omega^{ij}_{PM}(\phi)) D^2_{m'm}(\Omega_{MR}) \times d^2_{m0}(\beta_{RL})\exp(-im\omega_r t), \quad (3)$$

with P^{ij} denoting the principal axis of the dipole–dipole interaction between spins i and j, and M, R, and L denoting the molecular, the rotor, and the laboratory frame, respectively. $D^2_{m'm}(\Omega_{AB})$ and $d^2_{m'm}(\beta_{AB})$ are the full and reduced Wigner rotation matrix elements, ω_r is the sample rotation frequency, chosen to be $\omega_r/2\pi$ = 4000 Hz in this work, and $\beta_{RL} = \tan^{-1}\sqrt{2}$ is the magic angle. The dipole–dipole coupling strength is given by $b_{ij} = -(\mu_0/4\pi)\gamma_i\gamma_j\hbar r_{ij}^{-3}$, with r_{ij} the internuclear distance. The P^{ij} frame has a z axis defined by the internuclear ^1H–^{13}C vector, and is thus specific to a particular ^1H–^{13}C pair. The z and x axes of the molecular frame M

TABLE 1 Bond lengths and angles in nucleoside-like H3′–C3′–C4′–H4′ moieties, determined by neutron diffraction

CSD designation*	R (%)	C3′–C4′ Distance (pm)	H3′–C3′ Distance (pm)	H4′–C4′ Distance (pm)	H3′–C3′–C4′ Angle (°)	H4′–C4′–C3′ Angle (°)	Reference
adenos01	4.4	151.6	95.3	102.8	112.40	109.34	Klooster et al., 1991
juqset01 (a)	6.4	154.4	109.0	111.4	109.40	108.78	Evdokimov et al., 1999
juqset01 (b)	6.4	153.0	110.5	110.6	108.91	109.21	Evdokimov et al., 1999
nruram11	3.3	153.6	109.9	109.2	111.69	110.08	Takusagawa et al., 1979
zowjaw01 (a)	11.8	153.1	110.6	108.7	111.69	110.45	Evdokimov et al., 1999
zowjaw01 (b)	11.8	154.1	108.9	111.4	109.50	111.14	Evdokimov et al., 1999
zozvuf	4.6	151.6	95.3	102.8	112.40	109.34	Singh et al., 1996
Average value		153.1	105.6	108.1	110.9	109.8	
Standard deviation		1.1	7.1	3.8	1.5	0.8	

*All entries are taken from the Cambridge Structural Database (www.ccdc.cam.ac.uk).

are along the C3′–C4′ bond and in the H3′–C3′–C4′ plane, respectively. The z axis of the R frame is along the rotor long axis, and the z axis of the L frame is along the static magnetic field. The reference frames are discussed in more detail in Ravindranathan et al. (2000).

The structurally interesting information lies in the relation between the P and M frames. For the H3′–C3′–C4′–H4′ fragment, we have,

$$\beta_{PM}^{H3'C3'} = \theta_{H3'C3'C4'} \tag{4a}$$

$$\beta_{PM}^{H4'C4'} = \pi - \theta_{H4'C4'C3'} \tag{4b}$$

$$\gamma_{PM}^{H3'C3'} - \gamma_{PM}^{H4'C4'} = \gamma_{PM}^{H3'C4'} - \gamma_{PM}^{H4'C3'} = \phi \tag{4c}$$

where θ_{ijk} are bond angles and ϕ is the H3′–C3′–C4′–H4′ torsional angle. In addition, the signal from the HCCH-2Q-HLF experiment depends on the scaling factor κ of the homonuclear decoupling sequence. We used FSLG decoupling, for which the theoretical value is 0.577 at maximum ^{1}H–^{1}H decoupling efficiency (Bielecki et al., 1989). In practice, we are able to fit this parameter at the same time as deriving the geometrical information (see below).

Estimation of the H3′–C3′–C4′–H4′ torsional angles

To estimate ϕ, the 2Q evolution function $f(t_1, \kappa, \phi)$ is calculated for a set of κ and ϕ values. Simulations at each value of (κ, ϕ) are fitted to the experimental points using the overall vertical scale A and the 2Q exponential damping rate constant λ as adjustable parameters. The simulations also require input of the relevant bond angles θ_{ijk} and bond lengths r_{ij}, see Eq. 4. These were set to the average values of a set of seven structures determined by neutron diffraction, as reported in the last row of Table 1. Note that the directly bonded ^{13}C–^{1}H distances used in the simulations were directly obtained from the neutron diffraction data and were not corrected for vibrational effects. This procedure impacts on the fitted values of the scaling factor κ, as discussed below.

Before analyzing the experimental data, it is important to establish the significance of remote protons on the 2Q evolution curves. The dashed lines in Fig. 5 show 2Q evolution curves simulated as a function of the torsional angle ϕ, including only the four spins in the local H3′–C3′–C4′–H4′ unit. The solid lines include the two H2′ protons, the two H5′ protons and the O3H′ proton as well as the four spins in the local H3′–C3′–C4′–H4′ unit. The additional protons were positioned using the structural parameters listed in Table 2. For simplicity, only interactions over a distance of 250 pm or less were included. As may be seen, the inclusion of the five remote protons has a small but significant effect on the simulated curves, particularly in the region of ϕ close to 180°. This is in contrast to a recent analysis of the 2Q evolution in bacteriorhodopsin, where the influence of remote protons was found to be negligible (Lansing et al., 2002).

The inclusion of remote protons complicates the analysis, because the locations of these protons depends on torsional angles outside the four-spin unit, and these torsional angles are not known a priori. However, it is possible to position the two H2′ protons as function of ϕ by assuming tetrahedral geometry at the C2′ carbon and by using the empirical relationship $\nu_2 \approx 0.0119\nu_3^2 - 0.8385\nu_3 - 25.99°$ between the furanose torsional angles C1′–C2′–C3′–C4′ (ν_2) and C2′–C3′–C4′–O4′ (ν_3), which is a good fit to the data presented in Saenger (1984). The position of the H5′ and O3H′ protons, in contrast, requires knowledge of the torsional angles γ and ε. Fortunately, it was verified by further simulations (not shown) that the values of γ and ε only have a small effect on the simulated curves (see below).

Figure 6 shows contour plots of the mean square deviation between experiment and simulation, χ^2, as a function of the scaling factors κ and the H3′–C3′–C4′–H4′ torsional angles ϕ, for $^{13}C_2$-dT (Fig. 6 *a*) and $^{13}C_2$-dC·HCl (Fig. 6 *b*).

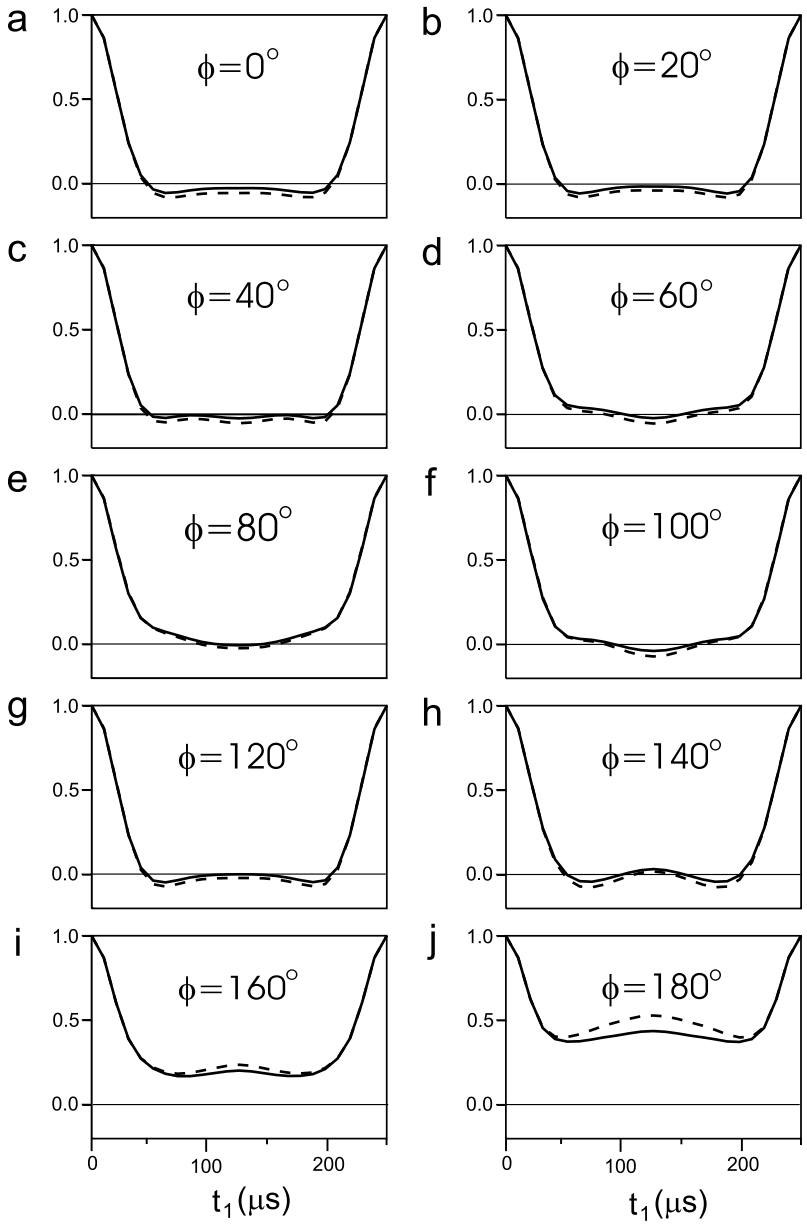

FIGURE 5 Theoretical functions $f(t_1, \kappa, \phi)$ for the H3′–C3′–C4′–H4′ fragment with (*solid line*) and without (*dashed line*) inclusion of the remote OH3′, H2′, and H5′ protons. The scaling factor was assumed to be $\kappa = 0.50$. The values of ϕ are indicated.

For each point in the (κ, ϕ) surface, a simulation was performed using the two ^{13}C spins and the five nearest protons, positioned using the procedure described above. The simulations for $^{13}C_2$-dT used the torsional angles $\gamma = 173°$ and $\varepsilon = 165°$ (Chekhlov 1995), whereas the simulations for $^{13}C_2$-dC·HCl used $\gamma = 46°$ and $\varepsilon = 71°$ (Subramanian and Hunt, 1970) (see Table 3). The simulation at each value of (κ, ϕ) was matched to the experimental points by adjusting the vertical scale A and the exponential decay constant λ to minimize χ^2.

TABLE 2 Additional bond lengths and angles from the set of neutron diffraction structures in Table 1

Distance	Average Value (pm)	Standard Deviation (pm)	Angle	Average Value (°)	Standard Deviation (°)
H2′–C2′	106.9	4.6	H2′–C2′–C3′	109.5	3.0
C2′–C3′	153.5	0.7	C2′–C3′–C4′	102.0	0.9
C3′–O3′	141.5	0.9	C3′–O3′–O3H′	110.4	2.5
O3′–O3H′	92.9	9.5	O3′–C3′–C4′	111.3	2.1
C4′–C5′	151.8	0.6	C3′–C4′–C5′	113.4	2.4
C5′–H5′	108.0	5.1	C4′–C5′–H5′	108.5	0.9

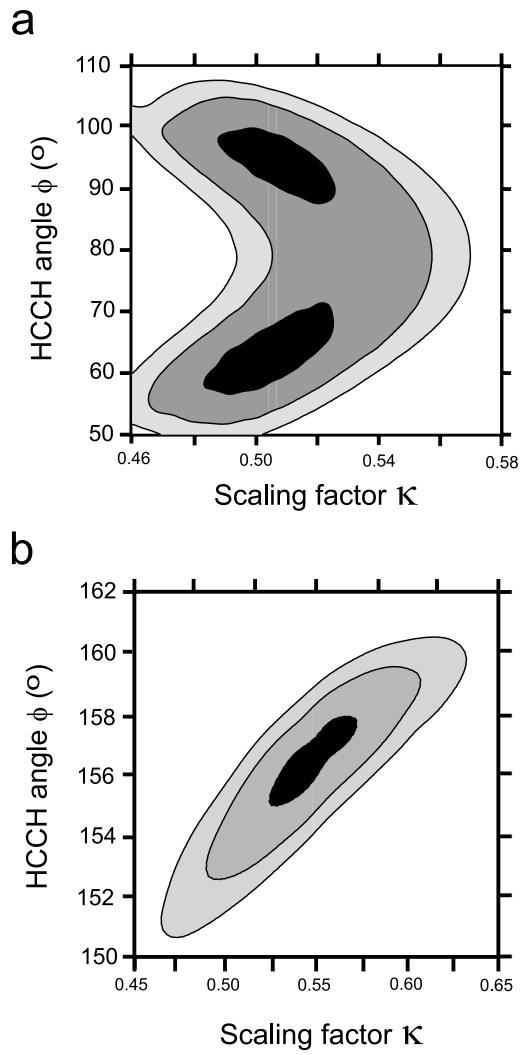

FIGURE 6 Contour plots of χ^2 versus the torsion angle ϕ and scaling factor κ for (*a*) [3′,4′-$^{13}C_2$]-thymidine and (*b*) [3′,4′-$^{13}C_2$]-2′-deoxycytidine·HCl. The analysis included ^{13}C dipole couplings to the H2′, H3′, OH3′, H4′, and H5′ protons (see Fig. 1). Distances and three-bond angles were set to the averages from neutron diffraction data, see Tables 2 and 3. The shaded regions are bounded by contours at $\chi^2 = \sqrt{2}\chi^2_{min}$, $2\sqrt{2}\chi^2_{min}$, and $3\sqrt{2}\chi^2_{min}$.

The plot for $^{13}C_2$-dT (Fig. 6 *a*) reveals two χ^2 minima at (κ, ϕ) = (0.51, 64°) and (0.51, 94°). In the case of $^{13}C_2$-dC·HCl (Fig. 6 *b*), a single χ^2 minimum is found at (κ, ϕ) = (0.54, 156°). The rather low values of κ found at these minima are probably due to the use of ^{13}C–^1H dipolar coupling constants that have not been corrected for vibrational motion.

There are also χ^2 minima at negative values of ϕ, with slightly different values of $|\phi|$. The χ^2 surface is not completely independent of the sign of ϕ, because the long-range interactions break the symmetry (Edén et al., 2000). In the following discussion, we only consider positive values of ϕ, because only these give rise to physically realistic values of the torsional angle δ (see below).

Figure 7 compares the experimental points with the best fit simulations at the global χ^2 minima (*solid lines*) for $^{13}C_2$-dT (Fig. 7 *a*) and $^{13}C_2$-dC·HCl (Fig. 7 *b*). In both cases, the fit between simulations and experimental points is very good. The residual deviations exceed the measured signal-to-noise ratio of the experimental points, which is too small to be shown on the plots. The residual deviations must therefore be attributed to the inaccuracy of the theoretical model, or experimental imperfections. Under these circumstances, the confidence limits on the parameters κ and ϕ may be determined by taking the boundary of the $\chi^2 = \sqrt{2}\chi^2_{min}$ contours (Press et al., 1994), which are shown as the darkest regions in Fig. 6. In the case of $^{13}C_2$-dT (Fig. 6 *a*) the contours indicate two ranges of ϕ yielding an acceptable fit between simulation and experiment, namely $\phi = 64° \pm 8°$ and $\phi = 94° \pm 6°$. In the case of $^{13}C_2$-dC·HCl (Fig. 6 *b*), the torsional angle estimate is $\phi = 156° \pm 2°$.

There are several additional factors that extend the confidence limits on ϕ. First, there is uncertainty in the precise values of the bond lengths and bond angles. Second, the simulations depend slightly on the remote torsional angles γ and ε, because these angles influence the location of the remote protons.

To assess the effect of the bond lengths and bond angles, 100 simulations were set up using bond lengths and bond angles of the H3′–C3′–C4′–H4′ fragment randomly distributed according to the average values and

TABLE 3 Structural data of thymidine and 2′-deoxycytidine·HCl from x-ray crystallography

	C3′–C4′ Distance (pm)	H3′–C3′ Distance (pm)	H4′–C4′ Distance (pm)	H3′–C3′–C4′ Angle (°)	H4′–C4′–C3′ Angle (°)	ϕ (°)	δ (°)	$\delta + \phi$ (°)	γ (°)	ε (°)
dT*	152.9	97.9	99.6	118.0	112.9	87.6	156.2	243.8	172.8	164.2
dT†	152.4	98.6	96.1	112.5	109.5	88.5	156.0	244.5	173.3	165.7
[3′,4′-$^{13}C_2$]-dT‡	152.4	100.0	100.0	112.2	109.2	88.5	157.0	245.5	172.4	168.5
dC·HCl§	151.7	100.6	96.0	109.9	110.4	161.0	81.4	242.4	46.2	70.7

*From Young et al. (1969).
†From Chekhlov (1995).
‡From Lutz et al. (2001).
§From Subramanian and Hunt (1970).

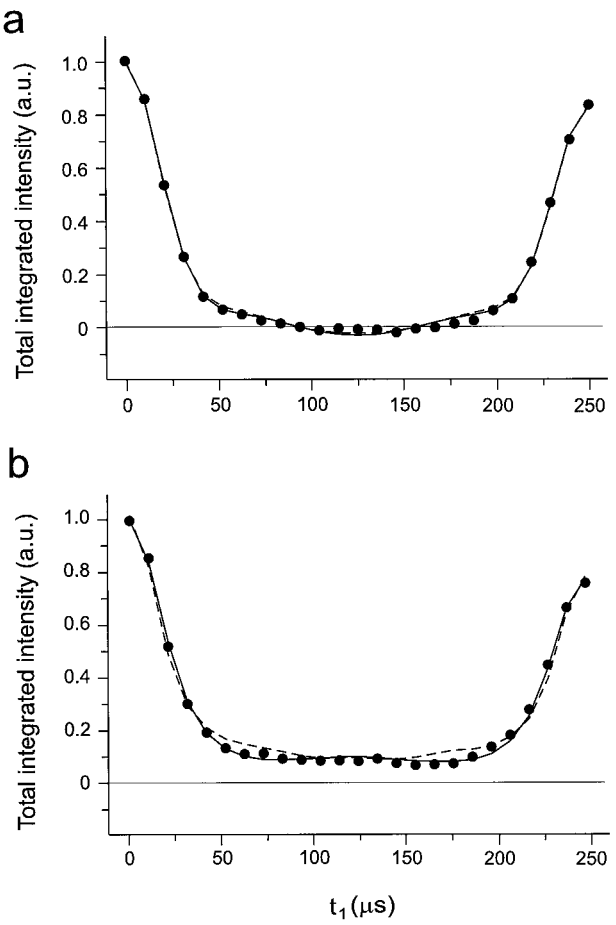

FIGURE 7 *Filled circles*, experimental points; *solid lines*, best fit simulated curves for (*a*) [3′,4′-$^{13}C_2$]-thymidine and (*b*) [3′,4′-$^{13}C_2$]-2′-deoxycytidine·HCl. The dashed lines show the best fit simulations with all distances and torsional angles set to the x-ray geometry as given in (Chekhlov, 1995) and (Subramanian and Hunt, 1970) (See also Table 3).

confidence limits shown in the last row of Table 1 (geometrical parameters outside the H3′–C3′–C4′–H4′ fragment were set to the average values from neutron diffraction data as reported in Table 2). A statistical analysis of the results showed that the uncertainty in the bond lengths and bond angles of the H3′–C3′–C4′–H4′ moiety contributes an additional 2.5° to the confidence limits of the determined ϕ angles.

To assess the effect of the γ and ε torsional angles, an ensemble of simulations was set up in which all nine combinations of (g^+, g^-, and t) for (γ, ε) were simulated. This had only a minor effect, adding another 1° of uncertainty to the determined values of ϕ. When all these factors are taken into account, the estimates of ϕ from the 2Q-HLF NMR experiments are $\phi = 64° \pm 8°$ and $\phi = 94° \pm 7°$ for $^{13}C_2$-dT and $\phi = 156° \pm 3°$ for $^{13}C_2$-dC·HCl.

In the case of $^{13}C_2$-dT, simulations involving only the four spins in the H3′–C3′–C4′–H4′ unit produced a single χ^2 minimum at $\phi = 72°$ rather than the double minimum shown in Fig. 6 *a*. The inclusion of remote protons is therefore essential in this case.

Estimation of δ and comparison with the x-ray structures

The H3′–C3′–C4′–H4′ torsional angle ϕ derived by the 2Q-HLF method is not of direct relevance to nucleic acid structure. More relevant is the C5′–C4′–C3′–O3′ torsional angle δ, which is indicative of the sugar puckering mode and has a strong effect on the disposition of adjacent nucleotides in a polynucleotide structure.

The ϕ and δ angles are related approximately through $\delta = 240° - \phi$, assuming tetrahedral bond geometries. An analysis of the seven neutron diffraction structures listed in Table 1 shows that the relation is better described as $\delta = 244° - \phi$ with a standard deviation of 4.2°. When this relationship is combined with the solid-state NMR estimations of ϕ, we obtain the following estimates of the δ torsional angle: $\delta = 179° \pm 9°$ or $150° \pm 8°$ for thymidine, and $\delta = 88° \pm 6°$ for 2′-deoxycytidine·HCl.

In the case of thymidine, the value $\delta = 179° \pm 9°$ represents an energetically unfavorable high C3′-exo conformation of the furanose ring. The estimate $\delta = 150° \pm 8°$, in contrast, represents the normally encountered C2′-endo conformation, which is ~8.4 kJ mol^{-1} more stable than the high C3′-exo conformation. On these grounds, we discard the high energy conformation and state the sugar pucker in our thymidine sample to be $\delta = 150° \pm 8°$.

In the case of 2′-deoxycytidine·HCl, the torsional angle estimate $\delta = 88° \pm 6°$ represents a low energy C3′-endo sugar puckering mode, tending toward O4′-endo at the higher end of the range.

The estimates of δ from 2Q solid-state NMR agree well with the structures of thymidine and 2′-deoxycytidine·HCl determined by x-ray crystallography, see Table 2. The x-ray estimate of δ for thymidine is 156°, which falls within the confidence limits for the 2Q-HLF measurements, namely $\delta = 150° \pm 8°$. For 2′-deoxycytidine·HCl, the x-ray estimate of $\delta = 81°$ falls just outside the 2Q-HLF confidence limits, $\delta = 88° \pm 6°$. We conclude that the two methods for molecular structure determination are in reasonable agreement, in the case of the heavy atom torsional angles.

Comparison of ϕ angles derived by NMR and x-ray diffraction

Although the values of δ determined by solid-state NMR and x-ray are in very good agreement for dT, and in reasonable agreement for dC·HCl, the values of ϕ estimated by the two methods appear not to be. The values of ϕ reported in the x-ray structures are shown in Table 1, and are in discrepancy with the solid-state NMR estimates of ϕ by as much as 11°.

It is possible to cross-check this conclusion by performing simulations with all relevant atoms positioned according to the x-ray coordinates, including the hydrogen atoms. In each case, the vertical scale factor A, damping rate constant λ, and multiple-pulse scaling factor κ are adjusted to minimize the deviation between experiment and simulation. The results are shown by the dashed lines in Fig. 7. For $^{13}C_2$-dT, the x-ray coordinates give a good fit to the experimental NMR data (Fig. 7 *a*), whereas for $^{13}C_2$-dC·HCl, the x-ray atomic positions give significant discrepancies with the experimental solid-state NMR data (Fig. 7 *b*).

There are three possible explanations for this behavior: 1) Both physical methods are influenced by vibrational motions, but in different ways. Thermal motions could lead to apparently different locations of the light hydrogen atoms determined by NMR and by x-ray diffraction; 2) the center of the hydrogen electron density determined by x-ray diffraction may not coincide with the proton positions; and 3) the accurate location of hydrogen atoms by x-ray diffraction is notoriously difficult, whereas both NMR and neutron diffraction are highly sensitive to proton positions. Note that, in the analysis reported above, the torsional angles δ were estimated by using NMR data for ϕ, combined with neutron diffraction data for estimating the relationship between ϕ and δ. Both NMR and neutron diffraction are considered to be reliable tools for locating the positions of protons. The result of this combined analysis leads to values for the heavy-atom torsional angles δ which are in agreement with the x-ray estimates. It therefore seems possible that the proton positions do not coincide exactly with the hydrogen atom locations reported in the x-ray studies, or that the confidence limits on the hydrogen atom positions have been underestimated.

CONCLUSIONS

These investigations have shown that the 2Q-HLF NMR method is a potentially useful method for the investigation of nucleic acid sugar pucker. However, it is necessary to include remote protons in the analysis, at least up to a distance range of 250 pm. Although our results for the sugar pucker angle δ are in good agreement with x-ray studies for both thymidine and 2′-deoxycytidine·HCl, there are significant discrepancies for the H3′–C3′–C4′–H4′ torsional angle ϕ, which could be associated with the difficulties of locating the protons by x-ray diffraction.

The experiment should be feasible on macromolecular systems that are beyond the reach of x-ray diffraction or solution NMR. In its simplest form, the method is restricted to systems with well-defined local conformations, but we anticipate that the method may be extended, in suitable cases, to systems that possess a distribution of torsional angles. This might involve combining the 2Q evolution with the conformational information contained in broadened chemically-shifted lineshapes (Zhang et al., 1998).

The authors thank Dr. Peter J. M. Verdegem for preliminary NMR work and Jasper R. Plaisier for participation in the x-ray diffraction measurements. Dr. Marjan Steenweg is thanked for help with the synthesis of 2′-deoxycytidine·HCl.

This work was sponsored by the Göran Gustafsson foundation for Research in the Natural Sciences and Medicine. We are grateful to Prof. Dr. J. Lugtenburg and Prof. Dr. J. H. van Boom for their participation in this investigation.

REFERENCES

Alam, T., and G. P. Drobny. 1991. Solid-state NMR studies of DNA structure and dynamics. *Chem. Rev.* 91:1545–1590.

Altona, C. 1982. Conformational analysis of nucleic acids. Determination of backbone geometry of single-helical RNA and DNA in aqueous solution. *Recl. Trav. Chim. Pays-Bas.* 101:413–433.

Bielecki, A., A. C. Kolbert, and M. H. Levitt. 1989. Frequency-switched pulse-sequences: homonuclear decoupling and dilute spin NMR in solids. *Chem. Phys. Lett.* 155:341–346.

Boisbouvier, J., B. Brutscher, A. Pardi, D. Marion, and J.-P. Simorre. 2000. NMR determination of sugar puckers in nucleic acids from CSA-dipolar cross-correlated relaxation. *J. Am. Chem. Soc.* 122:6779–6780.

Bower, P. V., N. Oyler, M. A. Metha, J. R. Long, P. S. Stayton, and G. P. Drobny. 1999. Determination of torsion angles in proteins using solid state NMR. *J. Am. Chem. Soc.* 121:8373–8375.

Cambridge Structural Database. The Cambridge Crystallographic Center, www.ccdc.cam.ac.uk.

Chekhlov, A. N. 1995. Intramolecular C–H···O interactions in the main nucleosides from crystallographic data. Refinement of the crystal structure of thymidine. *Zh. Strukt. Khim.* 36:178–184.

Cheng, V. B., H. H. Suzukawa, and M. Wolfsberg. 1973. Investigations of a nonrandom numerical method for multidimensional integration. *J. Chem. Phys.* 59:3992–3999.

Costa, P. R., J. D. Gross, M. Hong, and R. G. Griffin. 1997. Solid-state NMR measurement of ψ in peptides: a NCCN 2Q-heteronuclear local field experiment. *Chem. Phys. Lett.* 280:95–103.

Davies, D. B. 1978. Conformations of nucleosides and nucleotides. *Prog. Nucl. Magn. Reson. Spectrosc.* 12:135–225.

Edén, M., A. Brinkmann, H. Luthman, L. Eriksson, and M. H. Levitt. 2000. Determination of molecular geometry by high-order multiple-quantum evolution in solid-state NMR. *J. Magn. Res.* 144:266–279.

Evdokimov, A. G., A. J. Kalb, T. F. Koetzle, W. T. Klooster, and J. M. L. Martin. 1999. Structures of furanosides: density functional calculations and high-resolution x-ray and neutron diffraction crystal structures. *J. Phys. Chem.* A 103:744–753.

Felli, I. C., C. Richter, C. Griesinger, and H. Schwalbe. 1999. Determination of RNA sugar pucker mode from cross-correlated relaxation in solution NMR spectroscopy. *J. Am. Chem. Soc.* 121:1956–1957.

Feng, X., A. Brinkmann, H. Luthman, L. Eriksson, A. Gräslund, O. N. Antzutkin, and M. H. Levitt. 1998. Direct determination of a peptide torsional angle ψ by double-quantum solid-state NMR. *J. Am. Chem. Soc.* 119:12006–12007.

Feng, X., Y. K. Lee, D. Sandström, M. Edén, H. Maisel, A. Sebald, and M. H. Levitt. 1996. Direct determination of a molecular torsional angle by solid-state NMR. *Chem. Phys. Lett.* 257:314–320.

Feng, X., P. J. E. Verdegem, M. Edén, D. Sandström, Y. K. Lee, P. Bovee-Guerts, W. J. de Grip, J. Lugtenburg, H. J. M. de Groot, and M. H. Levitt. 2000. Determination of a molecular torsional angle in the metarhodopsin-I photointermediate of rhodopsin by double-quantum solid-state NMR. *J. Biomol. NMR.* 16:1–8.

Feng, X., P. J. E. Verdegem, Y. K. Lee, D. Sandström, M. Edén, P. Bovee-Guerts, W. J. de Grip, J. Lugtenburg, H. J. M. de Groot, and M. H. Levitt. 1997. Direct determination of a molecular torsional angle in the membrane protein rhodopsin by solid-state NMR. *J. Am. Chem. Soc.* 119:6853–6857.

Fujiwara, T., T. Shimomura, and H. Akutsu. 1997. Multidimensional solid-state nuclear magnetic resonance for correlating anisotropic interactions under magic-angle spinning conditions. *J. Magn. Res.* 124: 147–153.

Gorenstein, D. G. 1992. ^{31}P NMR of DNA. *Methods Enzymol.* 211: 254–286.

Gregory, D. M., M. A. Mehta, J. C. Shiels, and G. P. Drobny. 1997. Determination of local structure in solid nucleic acids using double quantum nuclear magnetic resonance spectroscopy. *J. Chem. Phys.* 107:28–42.

Hohwy, M., H. J. Jakobsen, M. Edén, M. H. Levitt, and N. C. Nielsen. 1998. Broadband dipolar recoupling in the nuclear magnetic resonance of rotating solids: a compensated C7 pulse sequence. *J. Chem. Phys.* 108:2686–2694.

Hong, M., J. D. Gross, and R. G. Griffin. 1997. Site-resolved determination of peptide torsion angle ϕ from the relative orientations of backbone N–H and C–H bonds by solid-state NMR. *J. Phys. Chem. B.* 101: 5869–5874.

Ippel, J. H., S. S. Wijmenga, R. de Jong, H. A. Heus, C. W. Hilbers, E. de Vroom, G. A. van der Maarel and J. H. van Boom. 1996. Heteronuclear scalar couplings in the bases and sugar rings of nucleic acids: their determination and application in assignment and conformational analysis. *Magn. Reson. Chem.* 34:156–176.

Ishii, Y., T. Terao, and M. Kainosho. 1996. Relayed anisotropy correlation NMR: determination of dihedral angles in solids. *Chem. Phys. Lett.* 256:133–140.

Klooster, W. T., J. R. Ruble, B. M. Craven, and R. K. McMullan. 1991. Structure and thermal vibrations of adenosine from neutron diffraction data at 123 K. *Acta Cryst.* 47:376–383.

Lansing, J. C., M. Hohwy, C. P. Jaroniec, A. F. L. Creemers, J. Lugtenburg, J. Herzfeld, and R. G. Griffin. 2002. Chromophore distortions in the bacteriorhodopsin photocycle: evolution of the H–C14–C15-H dihedral angle measured by solid-state NMR. *Biochemistry.* 41:431–438.

Lee, S. A., H. Grimm, W. Pohle, W. Scheiding, L. van Dam, Z. Song, M. H. Levitt, N. Korolev, A. Szabo, and A. Rupprecht. 2000. The NaDNA.bipyridyl(ethylendiamine)platinum(II) complex: I. Structure in oriented wet-spun films and fibers. *Phys. Rev. E.* 62:7044–7058.

Lee, Y. K., N. D. Kurur, M. Helmle, O. G. Johannessen, N. C. Nielsen, and M. H. Levitt. 1995. Efficient dipolar recoupling in the NMR of rotating solids. A sevenfold symmetric radiofrequency pulse sequence. *Chem. Phys. Lett.* 242:304–309.

Leupin, W., G. Wagner, W. A. Denny, and K. Wüthrich. 1987. Assignment of the ^{13}C nuclear magnetic resonance spectrum of a short DNA-duplex with ^{1}H-detected two-dimensional heteronuclear correlation spectroscopy. *Nucleic Acids Res.* 15:267–275.

Lutz, M., A. L. Spek, and J. Raap. 2001. Communication to the Cambridge Structural Database, www.ccdc.cam.ac.uk. (CCDC 172667).

Metz, G., X. Wu, and S. O. Smith. 1994. Ramped-amplitude cross polarization in magic-angle-spinning NMR. *J. Magn. Res.* 110:219–227.

Middleton, D. A., C. S. Le Duff, X. Peng, and D. G. Reid. 2000. Molecular conformations of the polymorphic forms of cimetidine from ^{13}C solid-state NMR distance and angle measurements. *J. Am. Chem. Soc.* 122: 1161–1170.

Ouwerkerk, N., M. Steenweg, M. de Ruijter, J. Brouwer, J. H. van Boom, J. Lugtenburg, and J. Raap. 2002. One-pot two-step enzymatic coupling of pyrimidine bases to 2-deoxy-D-ribose-5-phosphate. A new strategy in the synthesis of stable isotope labeled deoxynucleosides. *J. Org. Chem.* 67:1480–1489.

Ouwerkerk, N., J. H. van Boom, J. Lugtenburg, and J. Raap. 2000. Chemo-enzymatic synthesis of thymidine ^{13}C-labeled in the 2′-deoxyribose moiety. *Eur. J. Org. Chem.* 5:861–866.

Press, W. H., S. A. Teukolsky, W. T. Vetterling, and B. P. Flannery. 1994. Numerical Recipies. The Art of Scientific Computing. Cambridge University Press, Cambridge, U.K. 609–655.

Ravindranathan, S., X. Feng, T. Karlsson, G. Widmalm, and M. H. Levitt. 2000. Investigation of carbohydrate conformation in solution and in powders by double-quantum NMR. *J. Am. Chem. Soc.* 122:1102–1115.

Ravindranathan, S., T. Karlsson, K. Lycknert, G. Widmalm, and M. H. Levitt. 2001. Conformation of the Glycosidic Linkage in a Disaccharide Investigated by Double-Quantum Solid-State NMR. *J. Magn. Reson.* 151:136–141.

Rossi, P., and G. S. Harbison. 2001. Calculation of ^{13}C chemical shifts in RNA nucleosides: Structure-^{13}C chemical shift relationships. *J. Magn. Res.* 151:1–8.

Saenger, W. 1984. Principles of Nucleic Acid Structure. Springer-Verlag, New York.

Santos, R. A., P. Tang, and G. S. Harbison. 1989. Determination of the DNA sugar pucker using ^{13}C NMR spectroscopy. *Biochemistry.* 28: 9372–9377.

Schmidt-Rohr, K. 1996a. A double-quantum solid-state NMR technique for determining torsion angles in polymers. *Macromolecules.* 29: 3975–3981.

Schmidt-Rohr, K. 1996b. Torsion angle determination in solid ^{13}C-labeled amino acids and peptides by separated-local-field double-quantum NMR. *J. Am. Chem. Soc.* 118:7601–7603.

Singh, P., M. Zottola, S. Huang, B. R. Shaw, and L. G. Pedersen. 1996. 2′-deoxycytidine-*N*(3)-cyanoborane monohydrate. *Acta Cryst.* C52: 693–696.

Subramanian, E., and D. J. Hunt. 1970. The crystal structure and absolute configuration of 2′-deoxycytidine hydrocloride. *Acta Cryst.* B26: 303–311.

Takegoshi, K., T. Imaizumi, and T. Terao. 2000. One- and two-dimensional ^{13}C–^{1}H/^{15}N–^{1}H dipolar correlation experiments under fast magic-angle spinning for determining the peptide dihedral angle ϕ. *Solid State NMR.* 16:271–278.

Takusagawa, F., T. F. Koetzle, T. Srikrishnan, and R. Parthasarathy. 1979. C—H· · ·O interactions and stacking of water molecules between pyrimidine bases in 5-nitro-1-(β-D-ribosyluronic acid)-uracil monohydrate [1-(5-nitro-2,4-dioxopyrimidinyl)-β-D-ribofuranoic acid monohydrate]: a neutron diffraction study at 80 K. *Acta Cryst.* B35:1388–1394.

Travers, A. 1993. DNA–Protein Interactions. Chapman and Hall, London.

Tycko, R., D. P. Weliky, and A. E. Berger. 1996. Investigation of molecular structure in solids by two-dimensional NMR exchange spectroscopy with magic angle spinning. *J. Chem. Phys.* 105:7915–7930.

van Dam, L., and M. H. Levitt. 2000. BII nucleotides in the B and C-forms of natural-sequence polymeric DNA: a new model for the C-form of DNA. *J. Mol. Biol.* 304:541–561.

Weliky, D. P., and R. Tycko. 1996. Determination of peptide conformations by two-dimensional magic angle spinning NMR exchange spectroscopy with rotor synchronization. *J. Am. Chem. Soc.* 118:8487–8488.

Xu, X.-P., W.-L. A. K. Chiu, and S. C. F. Au-Yeung. 1998. Chemical shift and structure relationship in nucleic acids: correlation of backbone torsion angles γ and α with ^{13}C chemical shifts. *J. Am. Chem. Soc.* 120:4230–4231.

Young, D. W., P. Tollin, and H. R. Wilson. 1969. The crystal and molecular structure of thymidine. *Acta Cryst.* B25:1423–1432.

Zhang, P., A. N. Klymachyov, S. Brown, J. G. Ellington, and P. J. Grandinetti. 1998. Solid-state ^{13}C NMR investigation of the glycosidic linkage in α–α' trehalose. *Sol. State Nucl. Magn. Reson.* 12:221–225.